THE JOURNAL OF BIOLOGICAL CHEMISTRY VOL. 286, NO. 41, pp. 36011–36019, October 14, 2011
© 2011 by The American Society for Biochemistry and Molecular Biology, Inc. Printed in the U.S.A.

Vav Protein Guanine Nucleotide Exchange Factor Regulates CD36 Protein-mediated Macrophage Foam Cell Formation via Calcium and Dynamin-dependent Processes*

Received for publication, May 25, 2011, and in revised form, August 3, 2011 Published, JBC Papers in Press, August 24, 2011, DOI 10.1074/jbc.M111.265082

S. Ohidar Rahaman[‡1], **Gang Zhou**[‡], **and Roy L. Silverstein**[‡§2]

From the [‡]*Department of Cell Biology, Lerner Research Institute, Cleveland Clinic, Cleveland, Ohio 44195 and the* [§]*Department of Molecular Medicine, Cleveland Clinic Lerner College of Medicine, Cleveland, Ohio 44195*

Background: The scavenger receptor CD36 is known to activate Vav proteins, which function as GEFs for Rho GTPases and scaffolds for assembly of various signaling proteins.
Results: CD36-dependent activation of Vav proteins in macrophages by oxidized phospholipids was shown to trigger lipid uptake and foam cell formation by activating dynamin 2 and generating calcium signals.
Conclusion: Vav family GEFs regulate CD36-mediated oxLDL uptake and foam cell formation via calcium and dynamin 2-dependent processes.
Significance: Results from these studies will have therapeutic interest because small chemical inhibitors of dynamin GTPase activity or calcium antagonists may be useful as potential anti-atherosclerotic reagents.

Atherosclerosis, a chronic inflammatory disease, results in part from the accumulation of modified lipoproteins in the arterial wall and formation of lipid-laden macrophages, known as "foam cells." Recently, we reported that CD36, a scavenger receptor, contributes to activation of Vav-family guanine nucleotide exchange factors by oxidatively modified LDL in macrophages. We also discovered that CD36-dependent uptake of oxidized LDL (oxLDL) *in vitro* and foam cell formation *in vitro* and *in vivo* was significantly reduced in macrophages deficient of Vav proteins. The goal of the present study was to identify the mechanisms by which Vav proteins regulate CD36-dependent foam cell formation. We now show that a Vav-dynamin signaling axis plays a critical role in generating calcium signals in mouse macrophages exposed to CD36-specific oxidized phospholipid ligands. Chelation of intracellular Ca^{2+} or inhibition of phospholipase C-γ (PLC-γ) inhibited Vav activation (85 and 70%, respectively, compared with vehicle control) and reduced foam cell formation (approximately 75%). Knockdown of expression by siRNA or inhibition of GTPase activity of dynamin 2, a Vav-interacting protein involved in endocytic vesicle fission, significantly blocked oxLDL uptake and inhibited foam cell formation. Immunofluorescence microscopy studies showed that Vav1 and dynamin 2 colocalized with internalized oxLDL in macrophages and that activation and mobilization of dynamin 2 by oxLDL was impaired in *vav* null cells. These studies identified previously unknown components of the CD36 signaling pathway, demonstrating that Vav proteins regulate oxLDL uptake and foam cell formation via calcium- and dynamin 2-dependent processes and thus represent novel therapeutic targets for atherosclerosis.

The earliest atherosclerotic lesion, known as the fatty streak, is primarily composed of lipid-laden macrophages or "foam cells." A crucial step in foam cell formation is recognition and internalization of oxLDL[3] by scavenger receptors, including CD36 and scavenger receptor A (SR-A) (1). Cumulative results from our group and others demonstrated that CD36 accounts for a large proportion of foam cell formation *in vivo* and *in vitro* (2–6). However, the precise molecular mechanisms required for oxLDL uptake and macrophage foam cell formation are not fully understood. Notably, our newly published data revealed that CD36 contributes to activation of Vav family proteins in aortas from hyperlipidemic *apoe* null mice (7) and that oxLDL induces activation of macrophage Vav *in vitro* in a CD36 and Src family kinase-dependent manner (7). We also found that CD36-dependent uptake of oxLDL and foam cell formation was significantly reduced in macrophages deficient of Vav proteins (7). The studies outlined here uncover previously unknown mechanisms by which Vav proteins regulate oxLDL uptake and foam cell formation via calcium- and dynamin 2-dependent processes.

Vav family proteins are multidomain signal transduction molecules that primarily act as a guanine nucleotide exchange factors (GEF) for the Rho/Rac/Cdc42 family of small GTPases (8, 9). They also functions as adaptor platforms for various signaling proteins including dynamin, PLC-γ, ZAP70, Lyn, and Syk (8, 9). They are activated by ligation of several receptors, including the T-cell and B-cell

* This work was supported, in whole or in part, by National Institutes of Health Grant HL087018.
[1] To whom correspondence may be addressed. E-mail: rahamao@ccf.org.
[2] To whom correspondence may be addressed. E-mail: silverr2@ccf.org.

[3] The abbreviations used are: oxLDL, oxidatively modified LDL; apoE, apolipoprotein E; GEF, guanine nucleotide exchange factors; NO_2LDL, leukocyte myeloperoxidase/nitrite system; KOdiA-PC, 1-(palmitoyl)-2-(5-keto-6-octenedioyl) phosphatidylcholine; DiI, 1,1′-dioctadecyl-3,3,3′, 3′-tetramethylindocarbocyanine iodide; TFP, trifluoperazine; BAPTA/AM, *O,O*′-bis(2-aminophenyl)ethylene glycol-*N,N, N*′,*N*′-tetraacetic acid/tetraacetomethyl ester; MPM, mouse peritoneal macrophage(s); BMDM, bone marrow-derived macrophages; IP, immunoprecipitation; IB, immunoblot; SR-A, scavenger receptor A; PLC-γ, phospholipase C-γ; MPO, myeloperoxidase; CaM, calmodulin.

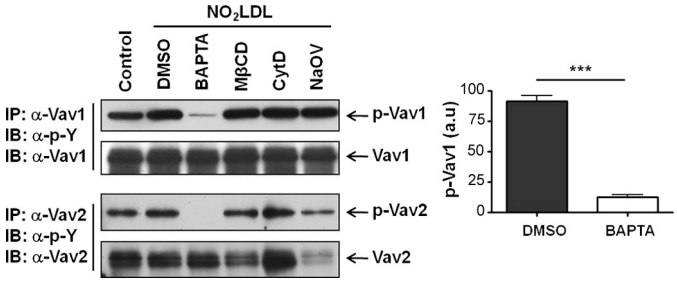

FIGURE 1. **Intracellular calcium regulates oxLDL-induced activation of Vav proteins in macrophages.** MPM pretreated with vehicle (*DMSO*), BAPTA/AM (5 μM), methyl-β-cyclodextrin (*MβCD*) (5 mM), cytochalasin-D (*CytD*) (20 μM), or sodium orthovanadate (NaOV) (20 μM) were exposed to NO_2LDL (50 μg/ml) and Vav activation status detected by IP followed by IB analysis. Cells without NO_2LDL treatment were used as control. In brief, whole cell extracts were subjected to IP with antibodies to the two specific Vav family members. Precipitates were then subjected to IB analysis with anti-phospho-tyrosine, and the blots were then stripped and reprobed with antibodies to the individual Vavs to assess total protein loaded. The *bar graphs* of mean ± S.E. from three separate experiments show an 85% decrease in Vav1 phosphorylation in the presence of BAPTA. ***, $p < 0.0001$, Student's *t* test. *DMSO*, dimethyl sulfoxide.

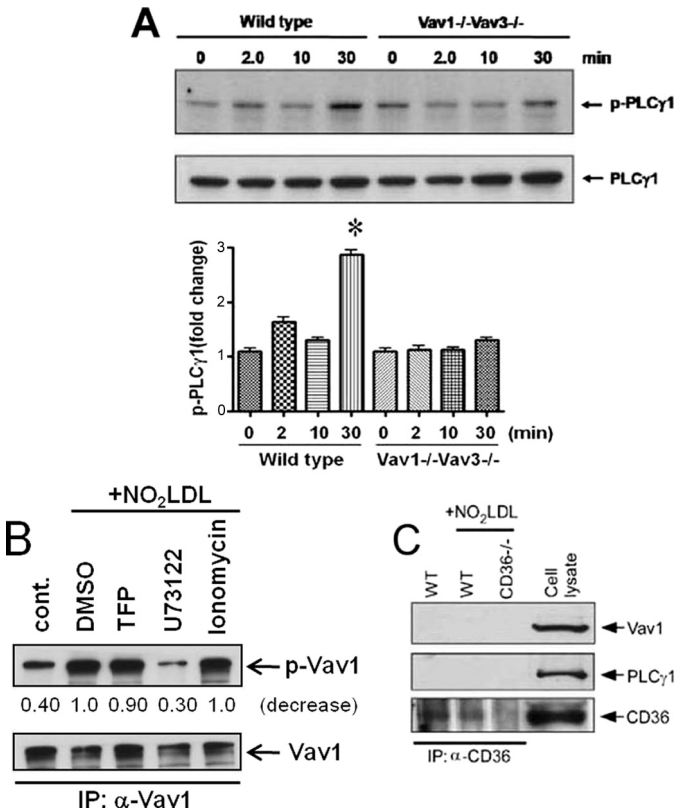

FIGURE 2. **PLCγ1 regulates oxLDL-induced activation of Vav proteins in macrophages.** *A*, IB of extracts from WT and *vav1;vav3* double-null MPM exposed to NO_2LDL for timed points using antibodies to PLC-γ1 and p-PLC-γ1 shows impaired phosphorylation in *vav* null cells compared with the WT. The *bar graphs* show mean ± S.E. from three separate experiments. *, $p < 0.05$, Student's *t* test. *B*, MPM pretreated with a PLCγ inhibitor (U73122, 1 μM), calmodulin inhibitor (TFP, 5 μM), or calcium ionophore (ionomycin, 5 μM) were exposed to NO_2LDL or untreated and assessed for Vav1 phosphorylation by IP/IB as in Fig. 1. The blot is representative of three separate experiments. *C*, WT and *cd36* null MPM were treated with NO_2LDL (50 μg/ml) for 2 min, and CD36 was immunoprecipitated with a monoclonal antibody. IPs were analyzed by IB with antibodies to Vav1, PLCγ1, and CD36. A cell lysate from WT MPM was used as a positive control.

antigen receptors, integrins, growth factor receptors, and chemokine receptors (8, 10–12). Considerable evidence supports a critical role for Vavs in receptor-dependent activation of MAP kinases (8, 13–15), generation of Ca^{2+} flux (8, 16–18) and reactive oxygen species (8, 19–21), cytoskeletal remodeling (8, 22–25), endocytosis (8, 21, 22), and migration in many cell types (8, 11, 26, 27). Among the three structurally and functionally related members of the Vav family, Vav1 is exclusively expressed in hematopoietic cells, whereas Vav2 and Vav3 are ubiquitously expressed.

Vav proteins have been linked to calcium responses via PLC-γ activation in many cell types (8, 16). It has also been reported that during T cell activation dynamin, a large GTPase, interacts with Vav1 and regulates PLCγ1 activation and Ca^{2+} mobilization (28, 29). Considerable evidence suggests that Ca^{2+} can increase endocytic vesicle size, accelerate membrane fission, and regulate endocytic membrane retrieval (30). These calcium-dependent processes may be critical during endocytosis of oxLDL, an early event in foam cell formation. Given that dynamin plays a critical role in endocytosis, it is rational to hypothesize that activation of a Vav-dynamin pathway can regulate foam cell formation via Ca^{2+}-dependent process. We now show that Vav plays an important role in activation of dynamin 2 and generation of calcium signaling in macrophages activated by CD36-specific oxidized phospholipid ligands. Mechanistically we show that dynamin-2 is essential for CD36-mediated foam cell formation, co-localizes with Vav1 and internalized oxLDL in macrophages, and mediates endocytosis of oxLDL-containing vesicles.

EXPERIMENTAL PROCEDURES

Antibodies, Cells, and Reagents—Antibodies to PLCγ1 and its phosphorylated form were from Cell Signaling Technology, Inc. (Beverly, MA). Antibodies to actin, Vav1, and Vav2 were from Santa Cruz Biotechnology, Inc. (Beverly, MA). Anti-dynamin2 antibody was from BD Transduction Laboratories. Rabbit anti-mouse CD36 antibody was from Dr. Huy Ong (University of Montreal, Canada). Anti-p-tyrosine clone 4G10 was from Upstate Biotechnology (Charlottesville, VA). KOdiA-PC (1-(palmitoyl)-2-(5-keto-6-octenedioyl) phosphatidylcholine) was from Cayman Chemical (Ann Arbor, MI). LDL was isolated from fresh human plasma as described previously and stored under N_2 gas until use. All LDL concentrations were expressed in terms of protein content as measured by Lowry assay. LDL oxidized by the leukocyte myeloperoxidase/nitrite system (NO_2LDL) was prepared as described previously (2). As controls for NO_2LDL, the LDL particles were incubated with the system in the absence of nitrite (-NO_2LDL). DiI (1,1′-dioctadecyl-3,3,3′,3′-tetramethylindocarbocyanine iodide) and fura-2/AM were from Molecular Probes (Eugene, OR), and U73122, TFP (trifluoperazine), ionomycin, BAPTA/AM (*O,O*′-bis(2-aminophenyl)ethylene glycol-*N,N, N*′,*N*′-tetraacetic acid/tetraacetomethyl ester) and dynasore were from Calbiochem (La Jolla, CA). The SMARTpool siRNA for mouse dynamin 2 and the non-targeted control siRNA were obtained from Dharmacon (Pittsburgh, PA). All other chemicals were obtained from Sigma unless indicated. *cd36*, *apoe*, *lyn*, and *fyn* null mice and *vav1;vav3* double-null mice were described previously. *vav1* null mice were provided by Dr. J. Rivera (National Institutes of Health, Bethesda,

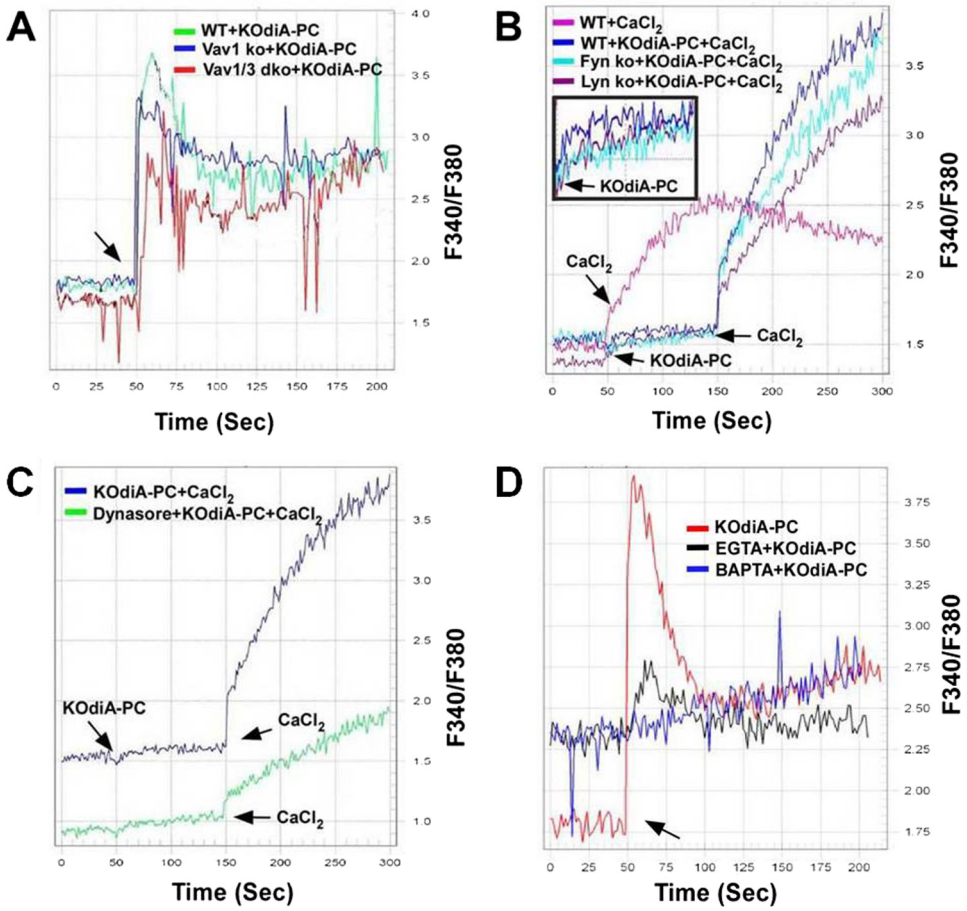

FIGURE 3. **OxPL induce macrophage Ca^{2+} flux in a Vav-dependent manner.** MPM (10^6 cells/ml) loaded with fura2-AM (4 μM) for 60 min were transferred to a cuvette, and fluorescence emission was recorded continuously at 340 and 380 nm after addition of KOdiA-PC (30 μg/ml). Intracellular Ca^{2+} was measured as above in WT, *vav1* null, and *vav1;vav3* double-null MPM (*A*) as well as *lyn* and *fyn* null MPM (*B*). The *inset* in Fig. 3*B* shows the basal level of Ca^{2+} flux generation in various cell types by KOdiA-PC in the absence of any external calcium. *C*, intracellular Ca^{2+} flux in MPM treated with dimethyl sulfoxide (*DMSO*) or the dynamin GTPase inhibitor dynasore (20 μM) for 30 min before stimulation with KOdiA-PC. In *B* and *C*, we compared calcium flux generation by KOdiA-PC because of influx of external calcium from added $CaCl_2$ (*arrows*). *D*, MPM pretreated with EGTA (2 mM) or BAPTA (10 μM) for 30 min were stimulated with KOdiA-PC (30 μg/ml) and intracellular Ca^{2+} measured as above. The *arrow* indicates the time of KOdiA-PC addition. Representative data from three experiments is shown.

MD). Mice were backcrossed at least six times to C57Bl/6 and background matched WT control lines were used in all studies. Thioglycollate-elicited mouse peritoneal macrophages (MPM) were isolated and maintained as described previously (5). Bone marrow-derived macrophages (BMDM) were derived from mouse bone marrow cells maintained in presence of macrophage colony-stimulating factor for 6–10 days.

Binding and Uptake of NO_2LDL—MPM were pretreated with inhibitors or vehicle for 30 min and then incubated with DiI-NO_2LDL (5 μg/ml) for 30 min at 4 °C to assess binding. Fluorescence intensity was examined by confocal or epifluorescence microscopy. To examine internalization, cells were then warmed to 37 °C and imaged at timed points up to 30 min. MPM harvested from *cd36* null mice were used to assess non-specific binding.

Foam Cell Assays—TG-elicited MPM from various strains were plated on coverslips in RPMI 1640 medium supplied with 10% FCS. After removing non-adherent cells, fresh medium was added and cells were maintained for 48h. MPM were then incubated with 50 μg/ml of NO_2LDL for 8 h in the presence or absence of various inhibitors in the same media. Cells were fixed with 4% formaldehyde, stained with Oil-Red-O, and foam cells were counted by microscopy. For the *in vivo* assays, TG-elicited MPM were collected from donor mice and 10^7 cells were then injected intraperitoneally into each recipient *apoe* null mouse maintained on a diet containing 0.15% cholesterol and 42% milk fat (TD88137, Harlan-Teklad) for 6 weeks. After 3 days, recipient mice were lavaged and cells analyzed as above by Oil-Red-O staining.

Immunoprecipitation (IP) and Immunoblot (IB) Analysis—For IP studies, cells were lysed in 20 mM Tris-HCl (pH7.5), 150 mM NaCl, 1 mM EDTA, 1 mM EGTA, 1% Nonidet P-40, 2.5 mM sodium pyrophosphate, 1 mM β-glycerophosphate, 1 mM Na_3VO_4, and 1 μg/ml leupeptide. The cleared supernatant containing 300–500 μg protein was incubated with 2–3 μg of antibody immobilized on agarose beads overnight at 4 °C. Beads were extensively washed in the same buffer and then boiled in SDS-PAGE loading buffer for subsequent IB. For CD36, coIP assays cells were treated with DSP (dithiobis-succinimidylpropionate) before harvesting in lysis buffer containing 1% CHAPS. Lysates were subject to IP using monoclonal anti-CD36 IgA and protein L-agarose. IBs were analyzed with a chemiluminescence detection system.

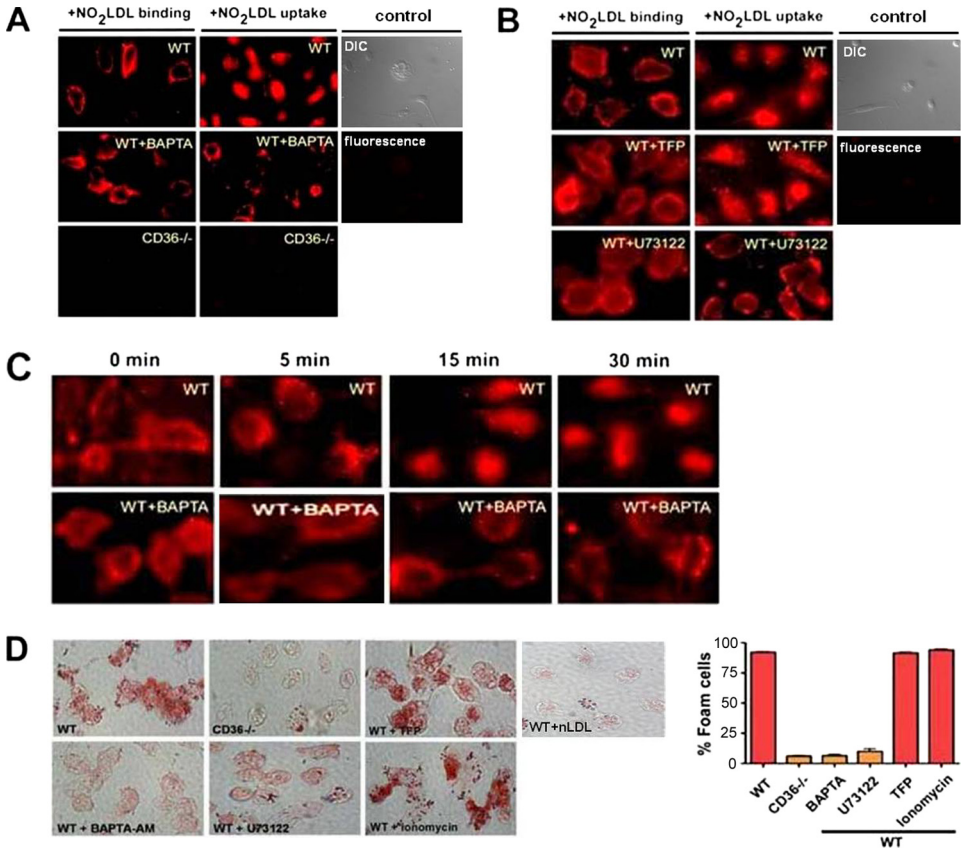

FIGURE 4. **CD36-mediated oxLDL uptake and foam cell formation are calcium-dependent.** *A* and *B*, MPM were pretreated with an intracellular calcium chelator (BAPTA/AM, 5 μM), PLCγ inhibitor (U73122, 1 μM), calmodulin inhibitor (TFP, 5 μM), or vehicle control for 30–60 min and then exposed to DiI-NO_2LDL (5 μg/ml) for 30 min at either 4 °C or 37 °C. Cells were examined by fluorescence microscopy to detect binding (4 °C) or uptake (37 °C). *cd36* null cells and WT cells not treated with DiI-NO_2LDL were used as a control. Differential interference contrast (*DIC*) and fluorescence images from WT control cells are shown. *C*, vehicle or BAPTA pretreated MPM were exposed to DiI-labeled NO_2LDL for 30 min at 4 °C to allow binding and then transferred to 37 °C to examine internalization at 0-, 5-, 15-, and 30-min intervals. *D*, MPM from WT or *cd36* null mice were treated with inhibitors as in *A* and *B* and then incubated for 8 h with 50 μg/ml of NO_2LDL. Cells were then fixed, stained with Oil-Red-O, and analyzed microscopically to quantify foam cell formation. WT cells exposed to native LDL are shown as control. The *bar graphs* show mean ± S.E. from four randomly chosen fields from each group.

Transfection of BMDM with siRNA—At day 6 of culture, BMDM were transfected with siRNA oligos using Accell siRNA delivery media according to the manufacturer's instructions (Dharmacon). After 72 h, cells were harvested for immunoblot analysis to examine knockdown efficacy and specificity.

Calcium Flux Analysis—Cells (2×10^6/ml) were loaded with 4 μM fura-2/AM in Hanks' balanced salt solution (with or without Ca^{2+}) for 60 min at 37 °C and then washed three times and diluted to 10^6/ml. Fluorescence was continuously monitored with a spectrophotometer with constant stirring using excitation at 340 and 380 nm and detecting emission at 510 nm. The ratio of 340/380 nm fluorescence was used to calculate intracellular Ca^{2+} concentration.

Fluorescence Microscopy—MPM were seeded on glass coverslips in RPMI 1640 medium with 10% FCS. After incubation with DiI-NO_2LDL (5 μg/ml) for timed points at 37 °C cells were fixed with 4% formaldehyde and incubated with primary antibodies. Alexa Fluor-coupled secondary antibodies were then applied and cells were analyzed by fluorescence microscopy.

RESULTS

PLC-γ1 and Ca^{2+} Are Necessary for Activation of Vavs in Macrophages—Because intracellular calcium flux (8, 16–18), actin polymerization (8, 22–25), lipid raft clustering (23, 24), and phosphatases (31) have been shown to participate in Vav activation in other systems, we examined the effect of selective pharmacologic inhibitors of these processes on CD36-mediated macrophage Vav activation. MPM pretreated with BAPTA/AM to chelate intracellular calcium, methyl-β-cyclodextrin to disrupt lipid rafts, cytochalasin-D to inhibit actin polymerization, or sodium orthovanadate to inhibit phosphatases were exposed to NO_2LDL (a highly specific ligand for CD36), and Vav phosphorylation was assayed by IP/IB. Cell viability measured by trypan blue exclusion was greater than 95% in all studies (data not shown). As shown in the representative blot in Fig. 1, Vav1 and Vav2 activation were blocked more than 85% by chelating intracellular calcium, whereas the other inhibitors had no effect. These data are consistent with previous reports that oxLDL can induce Ca^{2+} flux in leukocytes (32).

Because PLC-γ plays a critical role in intracellular calcium signaling, we next demonstrated by IB with an antibody specific to phospho-PLC-γ1 (Fig. 2*A*) that NO_2LDL induced a time-dependent increase in PLC-γ1 phosphorylation in MPM with a 3-fold increase seen at 30 min compared with the untreated control (*0′ min*). No increases were seen in MPM isolated from *vav1; vav3* double-null mice, showing that PLC-γ1 activation by oxLDL was Vav-dependent. Using specific pharmacologic inhibitors, we

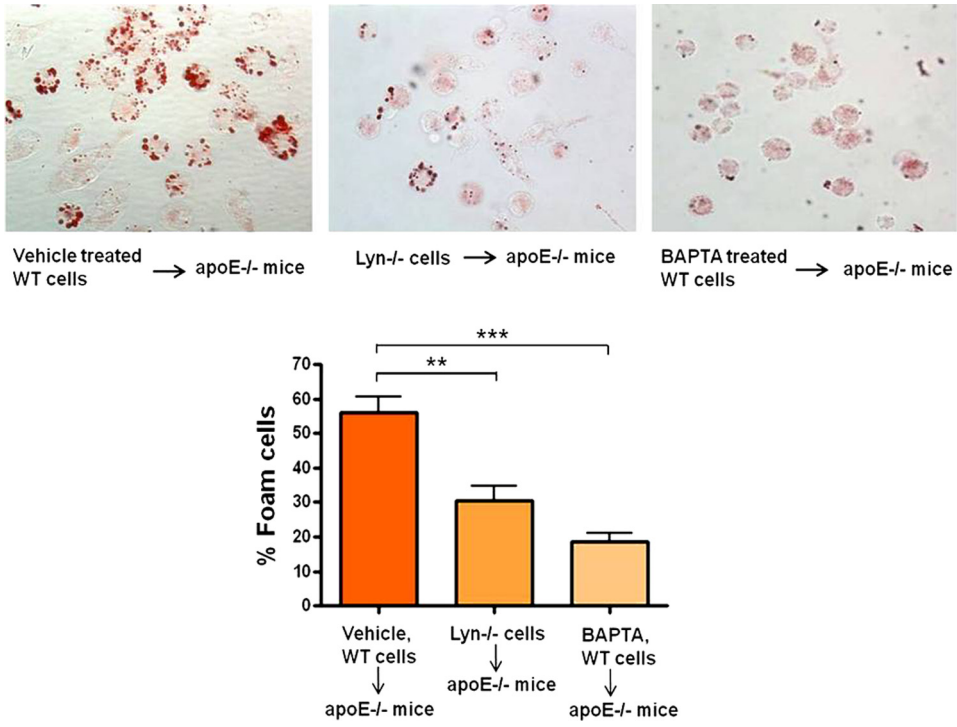

FIGURE 5. ***In vivo* foam cell formation is dependent on calcium flux and Src kinase Lyn.** BAPTA/AM- (5 μM) or dimethyl sulfoxide (*DMSO*)-pretreated WT cells and *lyn* null cells were injected intraperitoneally into *apoe* null recipient mice ($n = 3$ for each group) that had been maintained on a Western diet for 6 weeks. After 72 h, cells were recovered from the recipient mice and stained with Oil-Red-O to quantify foam cell formation. The *bar graphs* show mean ± S.E. from five randomly chosen fields from each group. **, $p < 0.005$; ***, $p < 0.0002$, Student's *t* test.

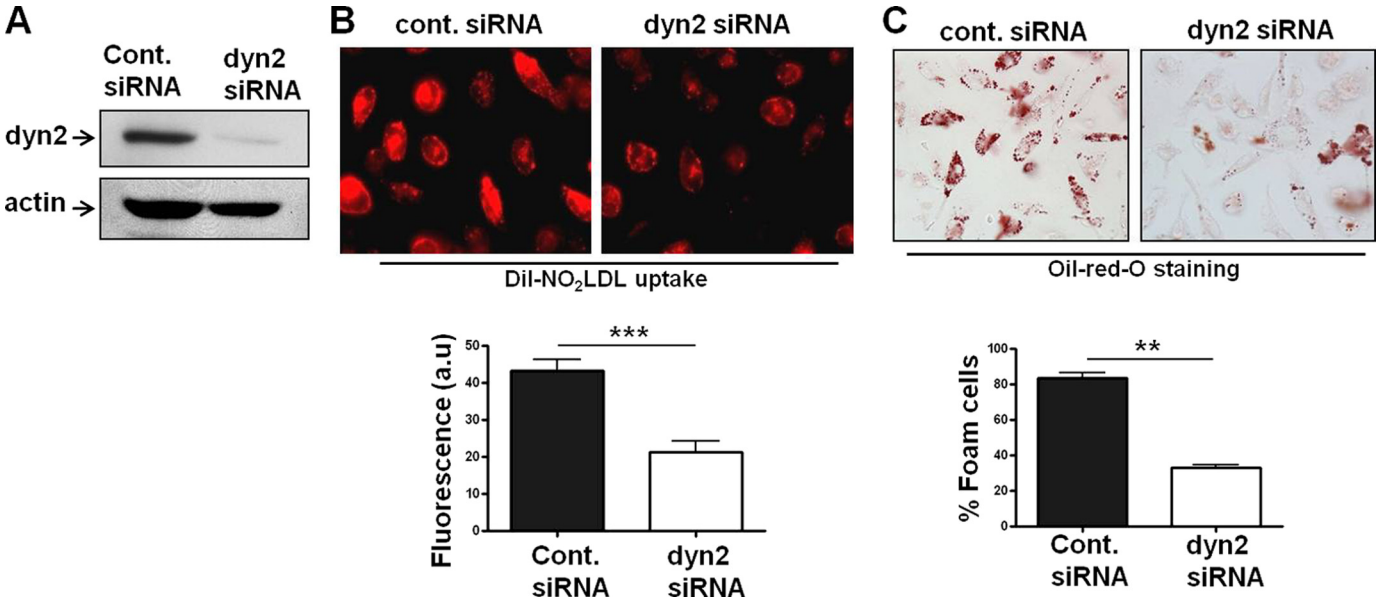

FIGURE 6. **CD36-mediated oxLDL uptake and foam cell formation are dependent on dynamin 2.** *A*, BMDM were transfected with control scramble or dynamin 2 siRNA duplex oligonucleotides for 72 h. Cell lysates obtained from siRNA-treated cells were immunoblotted with antibodies to dynamin 2 and actin to determine the knockdown efficacy and specificity. *B*, BMDM were transfected with control-siRNA or dyn2-siRNA for 72 h, and then DiI-NO_2LDL uptake was visualized as in Fig. 4*A*. The *bar graph* shows mean cellular fluorescence. For quantitation we measured the fluorescence intensity of 7–9 randomly selected cells from each group by ImageJ software. ***, $p < 0.0001$, Student's *t* test. *C*, BMDM were transfected as above prior to incubation for 15 h with 50 μg/ml NO_2LDL. Cells were then fixed and stained with Oil-Red-O to quantify foam cell formation. The *bar graphs* show the mean ± S.E. from four randomly chosen fields from each group. **, $p < 0.005$, Student's *t* test.

found that inhibition of PLC-γ1 by U73122 decreased CD36-mediated Vav phosphorylation by 70% (Fig. 2*B*), whereas TFP, a calmodulin inhibitor, or ionomycin, a calcium ionophore, had no effect, suggesting a reciprocal oxLDL-CD36-mediated activating mechanism involving Vav and PLC-γ1. Interestingly, neither PLC-γ1 nor Vav1 were coprecipitated with anti-CD36 antibody from MPM (Fig. 2*C*), suggesting that the role of CD36 was indirect.

OxPL-mediated Ca^{2+} Signaling Is Disrupted in Vav-deficient Macrophages—To test the hypothesis that Vavs mediate macrophage Ca^{2+} flux generated by CD36-oxLDL interactions,

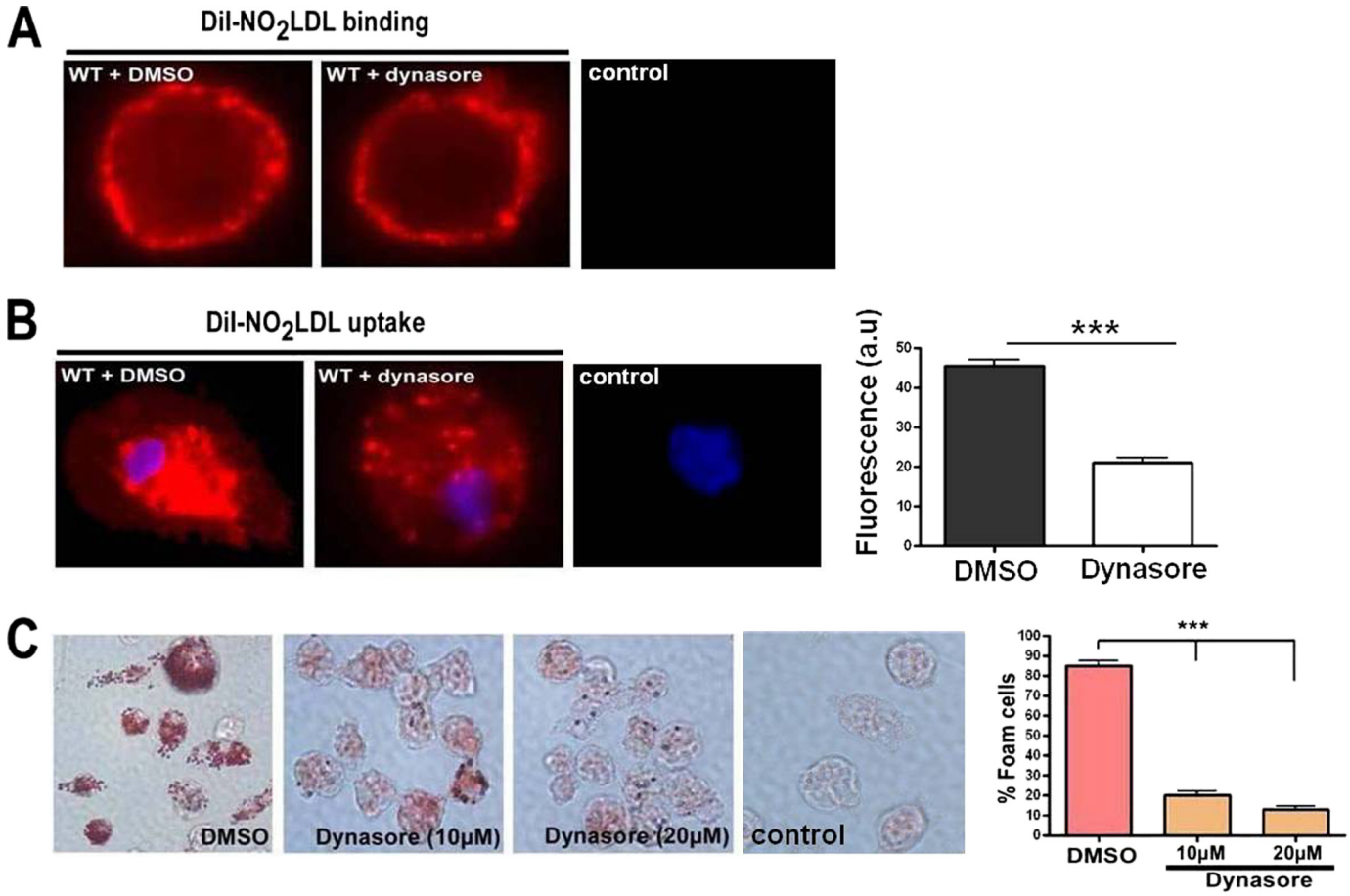

FIGURE 7. **CD36-mediated oxLDL uptake and foam cell formation are dependent on dynamin GTPase activity.** *A* and *B*, MPM were pretreated with an inhibitor of dynamin GTPase activity (dynasore, 10 μM) or vehicle for 60 min, and then DiI-NO_2LDL binding and uptake were visualized as in Fig. 4*A*. The *bar graph* shows mean cellular fluorescence for DiI-NO_2LDL uptake. For quantitation we measured fluorescence intensity of five to six randomly selected cells from each group by ImageJ software. ***, $p < 0.0001$, Student's *t* test. WT cells not treated with DiI-NO_2LDL are shown as a control. *C*, MPM were pretreated as above prior to incubation for 8 h with 50 μg/ml NO_2LDL. Cells were then fixed and stained with Oil-Red-O to quantify foam cell formation. The *bar graphs* show the mean± S.E. from four randomly chosen fields from each group. ***, $p < 0.0001$, Student's *t* test.

Fura2-AM loaded MPM were monitored by recording continuous fluorescence for 200–300 s after addition of CD36-specific oxidized phospholipid KOdiA-PC. To assess the roles of Vavs in this process, we compared Ca^{2+} flux in WT, *vav1* null, and *vav1;vav3* double-null MPM in response to KOdiA-PC. Basal levels of intracellular Ca^{2+} were similar in all of the cells (not shown) but although an increase in intracellular Ca^{2+} was seen in WT cells (Fig. 3*A*), *vav1;vav3* double-null cells showed approximately 50% less Ca^{2+} flux based on measured areas under the curve. *Vav1* null-cells showed a reduction in the early rapid rise, but the overall area under the curve was similar to the WT (Fig. 3*A*) perhaps because of compensation by Vav3. Because Vav activation by CD36 is regulated by Src family kinases (SFKs) (7) and because Ca^{2+} flux generation is an early event after oxPL-CD36 engagement, we also examined Ca^{2+} responses in MPM from *lyn* and *fyn* null mice. Fig. 3*B* shows that the KOdiA-PC-induced Ca^{2+} flux was moderately decreased in *fyn*- and *lyn* null cells compared with WT. Pretreatment of WT cells with KOdiA-PC before addition of $CaCl_2$ caused a marked increase in Ca^{2+} flux generation, possibly because of both internal and external sources of calcium. As shown in Fig. 3*B* (*inset*), in the absence of any external calcium source, a small but detectable rise of calcium flux by KOdiA-PC from intracellular stores was observed in WT cells, which supports this conclusion. Therefore, the robust increase in Ca^{2+} flux (Fig. 3*B*) after addition of $CaCl_2$ in KOdiA-PC-pretreated cells is attributed to both external and internal sources of calcium. Together, these data show that Vav activation, presumably via SFKs, may be involved in Ca^{2+} signaling by oxLDL-CD36 engagement in macrophages.

We also evaluated the role of dynamin, a Vav-interacting large GTPase known to regulate intracellular vesicle fission, in CD36-mediated Ca^{2+} flux generation. Dynasore, a specific dynamin GTPase inhibitor, markedly impaired the increase in intracellular Ca^{2+} induced by KOdiA-PC (Fig. 3*C*), suggesting that endocytic or phagocytic vesicle fission may be a source of Ca^{2+}. To further examine the source of the increase in Ca^{2+} flux we used EGTA to chelate extracellular calcium and BAPTA/AM to chelate intracellular calcium and found that BAPTA/AM completely inhibited the rise in intracellular Ca^{2+}, whereas EGTA inhibited it partially (Fig. 3*D*), suggesting that both intracellular and extracellular sources are responsible for CD36-generated Ca^{2+} flux. In the presence of EGTA, release of calcium from internal storage by addition of KOdiA-PC may have contributed to the observed rise in calcium flux. Altogether, these studies suggest a novel Ca^{2+}-dependent positive

feedback regulatory mechanism for activation of Vavs in macrophages. OxLDL-CD36 signaling induces Ca^{2+} flux via a SFK-Vav-PLCγ1 pathway, which is also essential for activation of Vavs by oxLDL.

Macrophage Ca^{2+} Flux Is Necessary for CD36-specific oxLDL Uptake and Foam Cell Formation—To address the pathophysiological importance of Ca^{2+} signaling in macrophages, we examined the binding and uptake of oxLDL by MPM treated with BAPTA/AM using NO_2LDL tagged with the fluorophore DiI. Equivalent binding was observed to both treated and untreated cells, but the uptake was nearly completely disrupted in cells treated with the BAPTA (Fig. 4*A*). U73122, a pharmacologic inhibitor of PLC-γ1, also severely disrupted the uptake of NO_2LDL without impacting binding (Fig. 4*B*), suggesting the possible involvement of PLC-γ1 activity in this process. Because Ca^{2+}-dependent association of calmodulin (CaM) with the inositol trisphosphate (IP_3) receptor can regulate calcium release from intracellular stores (33) and because the calponin homology domain of Vav1 has been shown to interact with CaM in T cells (17), we also assessed uptake and binding of NO_2LDL in the presence of TFP, a specific CaM inhibitor (Fig. 4*B*). A similar pattern of NO_2LDL binding and internalization was seen in vehicle and TFP-treated cells, suggesting a non-CaM-dependent mechanism involved in this process. Experiments were also performed by incubating cells with DiI-NO_2LDL for 30 min at 4 °C to allow surface binding and then transferring to 37 °C to measure uptake at timed points to 30 min. As before, no significant differences in binding were seen but uptake was severely impaired throughout the 30-min warm phase in BAPTA/AM-treated cells (Fig. 4*C*).

We next assessed the role of calcium signaling in macrophage transformation into foam cells. NO_2LDL-induced foam cell formation was quantified by microscopy after Oil-Red-O staining of cells treated with BAPTA/AM, U73122, or TFP. Fig. 4*D* shows that intracellular calcium chelation or inhibition of PLC-γ1 activity caused up to 80% reduction in foam cell formation whereas inhibition of CaM activity had no significant effect. To examine the *in vivo* role of Ca^{2+} flux and Src kinase Lyn (which moderately regulates Ca^{2+} flux generation by oxLDL) in macrophage foam cell formation we used an *in vivo* foam cell assay involving transfer of BAPTA/AM-pretreated or *lyn* null MPM into the peritoneal cavities of hyperlipidemic, Western diet-fed, *apoe* null recipients. After 72 h, cells were recovered from the peritoneal cavities, and foam cells were quantified by Oil Red O staining. Results showed that *in vivo* foam cell formation was significantly impaired in both BAPTA-pretreated and *lyn* null macrophages (Fig. 5), suggesting a critical role of calcium signaling and Lyn kinase in this process.

Vav-Dynamin Interactions Play a Critical Role in CD36-dependent oxLDL Uptake and Foam Cell Formation via Regulating oxLDL-containing Endosomal Vesicle Trafficking—The Vav-binding mechanochemical enzyme dynamin is critically involved in fission of endosomes from the cell membrane during endocytosis and hence in receptor-mediated uptake of numerous ligands (28). Because of the defect in oxLDL-containing endocytic vesicle formation/maturation seen in *vav* null cells (7) we explored the role of dynamin in this system. Sun *et al.* (34) recently reported that CD36-mediated oxLDL uptake

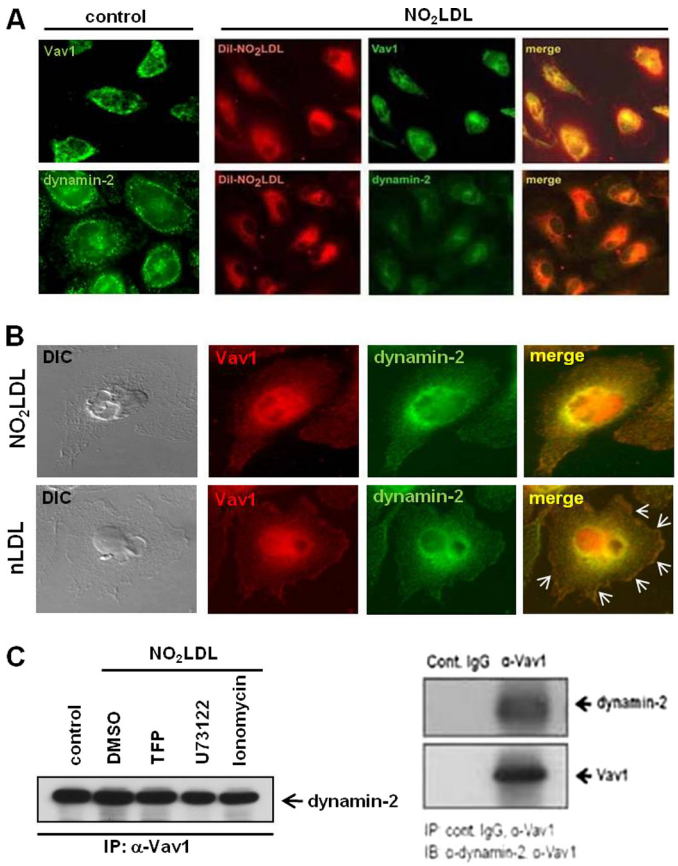

FIGURE 8. **Colocalization of Vav1 and dynamin-2 with internalized oxLDL in macrophages.** (A) MPM were incubated with DiI-NO_2LDL (5 μg/ml) for 30 min at 37 °C then fixed and incubated with monoclonal antibodies to Vav1 or dynamin-2 followed by Alexa 488-conjugated secondary antibody. Representative microscopic images of DiI-NO_2LDL (*red*), Vav1 (*green*), dynamin-2 (*green*), and merged (*yellow* or *orange*) are shown. *B*, MPM were incubated with NO_2LDL or nLDL (50 μg/ml) for 30 min at 37 °C then fixed and incubated with antibodies to Vav1 or dynamin 2 followed by Alexa Fluor-conjugated secondary antibodies. Representative microscopic images of Vav1 (*red*), dynamin-2 (*green*), merged (*yellow* or *orange*), and differential interference contrast (*DIC*) (*black and white*) are shown. Marked colocalization of Vav1 with dynamin 2 at plasma membrane areas are indicated by *arrows* in control cells treated with nLDL. *C*, Vav1 was immunoprecipitated from MPM (with or without NO_2LDL exposure) pretreated with dimethyl sulfoxide (*DMSO*), ionophore, U73122, or TFP (*left panel*). IPs were analyzed by IB with anti-dynamin 2 antibody. Cell extracts were immunoprecipitated with isotype-matched control IgG or antibody to Vav1 to show specificity of its interaction with dynamin 2 (*right panel*).

by transfected COS-7 cells is dependent on dynamin, and by using CD36/SRB1 chimeric protein constructs they found that the CD36 C-terminal cytoplasmic tail was necessary and sufficient for dynamin-dependent oxLDL internalization (34). To examine the role of dynamin 2 in primary macrophage foam cell formation, we transfected BMDM with dynamin2-siRNA (Fig. 6*A*) to knockdown dynamin 2 expression (the only form expressed in macrophages) and assessed DiI-NO_2LDL uptake. Fig. 6*B* shows a significantly reduced uptake of fluorescent NO_2LDL in dynamin 2-siRNA treated cells compared with control-siRNA. Consistent with these observations, dynamin 2-siRNA also significantly impaired foam cell formation in BMDM (Fig. 6*C*). To evaluate the specific role of dynamin GTPase activity in macrophage foam cell formation, we treated MPM with dynasore, an inhibitor of dynamin GTP hydrolysis and assessed DiI-NO_2LDL binding and uptake. Fig. 7*A* shows

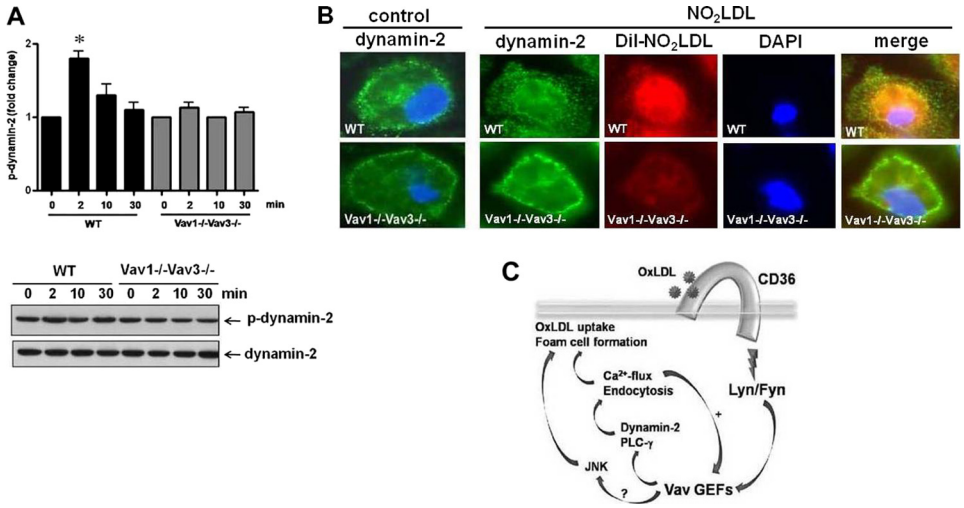

FIGURE 9. **Vav regulates oxLDL-mediated activation and translocation of dynamin 2.** *A*, MPM from WT and *vav1;vav3* double-null mice were exposed to NO_2LDL (50 μg/ml) for timed points to 30 min. Cell extracts were immunoprecipitated with antibody to dynamin 2, and precipitates were then subjected to immunoblot analysis with anti-p-tyrosine antibody. Blots were stripped and reprobed with antibody to dynamin 2 to assess total protein loaded. Blots were scanned to quantify band densities, and fold-change relative to total protein is indicated as mean ± S.E. $n = 3$. *, $p < 0.05$, Student's *t* test. *B*, untreated (*left panel*) and DiI-NO_2LDL-exposed (*right panel*) WT and *vav1;vav3* double-null MPM were stained as above with anti-dynamin 2 antibody (*green*). Nuclei were stained *blue* with DAPI. Merged images show impaired translocation of dynamin 2 to perinuclear areas in *vav1;vav3* double-null cells exposed to NO_2LDL (*right panel*). *C*, model depicting how oxLDL-CD36 engagement induces a signaling cascade that leads to recruitment and activation of the SFK Lyn, which in turn activates Vavs. Interaction of Vav proteins with PLCγ causes generation of Ca^{2+} flux, which in turn helps to maintain activation of Vavs, internalization of oxLDL, and formation of foam cells. Vavs also interact with dynamin 2, which plays a critical role in CD36-dependent oxLDL uptake and foam cell formation by regulating generation of Ca^{2+} flux and trafficking of the oxLDL-containing endosomes.

normal binding of NO_2LDL in the presence of dynasore but severe disruption of NO_2LDL uptake even after 30 min (Fig. 7*B*). Consistent with these observations, dynasore also impaired foam cell formation in MPM by approximately 85% (Fig. 7*C*).

To probe the mechanism by which dynamin 2 influences CD36-mediated oxLDL trafficking and foam cell formation, we used immunofluorescence confocal microscopy to first show that both Vav1 and dynamin 2 colocalized with internalized DiI-NO_2LDL in MPM (Fig. 8*A*). We also found that Vav1 and dynamin 2 fluorescence colocalized mainly in perinuclear areas in NO_2LDL treated cells compared with nLDL-treated (Fig. 8*B*). In native LDL (nLDL)-treated cells Vav1 and dynamin 2 colocalized on plasma membrane areas (*arrows*) as well as in perinuclear spaces. A direct interaction of Vav1 with dynamin 2 in macrophages *in vitro* was also demonstrated by coIP (Fig. 8*C*). No decreased interaction was seen comparing oxLDL-treated cells with U73122-treated or ionomycin-treated cells, suggesting that the Vav-dynamin interaction is constitutive; that is, not dependent on ligand engagement or Vav activation. As a negative control, we performed IP with isotype-matched control IgG (*right panel*). We also analyzed whether activation of dynamin 2 by oxLDL is mediated via the CD36-Vav signaling axis in macrophages. The results showed that stimulation of macrophages by NO_2LDL, a CD36-specific oxLDL, causes 1.8-fold increased phosphorylation of dynamin 2 in WT compared with *vav1;vav3* double-null cells (Fig. 9*A*). To determine whether dynamin 2 redistributes in response to oxLDL in a Vav-dependent manner, fluorescence microscopy was used to compare WT and *vav1;vav3* double-null MPM after exposure to DiI-NO_2LDL for 30 min. Translocation of dynamin 2 to perinuclear areas by NO_2LDL exposure was seen in WT cells but was impaired in *vav1;vav3* double-null cells (Fig. 9*B*, *right panel*), suggesting a regulatory role for Vavs in translocation of dynamin 2 during CD36-mediated endocytosis of oxLDL.

DISCUSSION

In this paper, we report that members of the Vav family of guanine nucleotide exchange factors regulate CD36-dependent foam cell formation via calcium and dynamin-dependent processes. Perhaps most significant is the critical role identified for dynamin 2, a Vav-interacting large molecular weight GTPase. Published studies have shown that Vavs regulate ligand-receptor endocytosis in other cell types (8, 21, 22), and indeed, we showed that *vav*-deficient macrophages had impaired maturation of oxLDL-containing endocytic vesicles and thus impaired ability to form foam cells (7). Dynamins are known to function in the fission of endocytic vesicles from the plasma membrane (28) and we found that dynamin-2 co-localized with oxLDL-containing vesicles during CD36-mediated endocytosis of oxLDL (Fig. 8). Furthermore, our siRNA-based studies revealed that dynamin 2 is required for uptake of CD36-specific oxLDL and macrophage foam cell formation (Fig. 6, *B* and *C*). On a mechanistic level, we demonstrated that dynamin GTPase activity is essential for efficient invagination and sorting of oxLDL-containing endosomes, key processes for transformation of macrophages to lipid-laden foam cells (Fig. 7). We also found that both Vav1 and dynamin 2 colocalized with internalized oxLDL in macrophages *in vitro* and provided biochemical data showing a direct interaction of Vav1 with dynamin-2 in macrophages (Fig. 8). Together, these data support the hypothesis recently put forward by Collins *et al.* (35) that CD36-mediated uptake is via a "conventional" endocytic pathway, rather than macropinocytosis. Our data, however, differ from those of Collins *et al.* in that we demonstrated that dynamin GTPase activity is necessary for CD36-mediated uptake, whereas they

did not see any effect with a dominant negative dynamin construct. This may relate to residual GTPase activity in cells transfected with the dominant negative construct or to differences in ligands utilized (CD36 antibodies *versus* NO_2LDL).

We also uncovered an important role for CD36-mediated calcium signaling in macrophage oxLDL uptake and foam cell formation (Figs. 4 and 5). It has been reported that during T cell activation, dynamin interacts with Vav1 and regulates PLCγ1 activation and Ca^{2+} mobilization (28, 29) and that in turn, dynamin function and trafficking can be regulated by Ca^{2+}. Because phagocytic vesicles can carry Ca^{2+} and dynamin plays a critical role during vesicle formation, it is likely that dynamin is playing a direct role in calcium signaling in macrophages in response to oxLDL (28, 29, 36). In many cells, Ca^{2+} increases endocytic vesicle size, accelerates membrane fission, and regulates endocytic membrane retrieval (30). Our studies also identified a novel Ca^{2+}-dependent positive feedback regulatory mechanism for Vav activation in macrophages. OxLDL-CD36 signaling induces Ca^{2+} flux via a SFK-Vav-PLCγ1 pathway, which is essential for activation of Vavs and dynamin 2 (Figs. 1, 2, 3, and 9). Vav and dynamin 2 then contribute to further Ca^{2+} flux generation in oxPL-exposed macrophages (Fig. 3). This is consistent with a recent report of an unbiased chemical screen that identified inhibitors of PLC-γ as modulators of oxLDL uptake by J774 monocytic cells (37). Interestingly, calcium antagonists have been shown to slow experimental atherosclerosis in animals and to suppress the generation of new lesions and the progression of existing lesions in humans (38).

In summary, we used a multipronged approach involving macrophages from a panel of genetically null mice along with specific inhibitors, highly specific oxidized phospholipid CD36 ligands, and *in vivo* and *in vitro* assays to identify mechanisms that bridge CD36 to downstream signaling events via Vav proteins. The model in Fig. 9*C* shows that oxLDL engagement with CD36 triggers SFK-dependent activation of Vav-GEFs, which results in activation of PLCγ1 and generation of a Ca^{2+} flux that mediates the sustained activation of Vav, the uptake of oxLDL, and the formation of foam cells. Activation of Vavs and the GTPase activity of its interacting partner, dynamin 2, play critical roles in macrophage foam cell formation via mechanisms regulating trafficking of oxLDL-containing endosomes. We found previously that CD36-dependent activation of JNK plays a critical role in macrophage oxLDL uptake and foam cell formation (6). It needs to be determined whether Vavs are involved in oxLDL-mediated activation of JNK in this model. These studies identified previously unknown components of the CD36-signaling pathway that are important in atherogenesis and thus represent novel targets for therapeutics.

REFERENCES

1. Glass, C. K., and Witztum, J. L. (2001) *Cell* **104,** 503–516
2. Podrez, E. A., Febbraio, M., Sheibani, N., Schmitt, D., Silverstein, R. L., Hajjar, D. P., Cohen, P. A., Frazier, W. A., Hoff, H. F., and Hazen, S. L. (2000) *J. Clin. Invest.* **105,** 1095–1108
3. Podrez, E. A., Poliakov, E., Shen, Z., Zhang, R., Deng, Y., Sun, M., Finton, P. J., Shan, L., Febbraio, M., Hajjar, D. P., Silverstein, R. L., Hoff, H. F., Salomon, R. G., and Hazen, S. L. (2002) *J. Biol. Chem.* **277,** 38517–38523
4. Zhao, Z., de Beer, M. C., Cai, L., Asmis, R., de Beer, F. C., de Villiers, W. J., and van der, Westhuyzen, D. R. (2005) *Arterioscler. Thromb. Vasc. Biol.* **25,** 168–173
5. Febbraio, M., Podrez, E. A., Smith, J. D., Hajjar, D. P., Hazen, S. L., Hoff, H. F., Sharma, K., and Silverstein, R. L. (2000) *J. Clin. Invest.* **105,** 1049–1056
6. Rahaman, S. O., Lennon, D. J., Febbraio, M., Podrez, E. A., Hazen, S. L., and Silverstein, R. L. (2006) *Cell Metab.* **4,** 211–221
7. Rahaman, S. O., Swat, W., Febbraio, M., and Silverstein, R. L. (2011) *J. Biol. Chem.* **286,** 7010–7017
8. Bustelo, X. R. (2001) *Oncogene* **20,** 6372–6381
9. Swat, W., and Fujikawa, K. (2005) *Immunol. Res.* **32,** 259–265
10. Turner, M., and Billadeau, D. D. (2002) *Nat. Rev. Immunol.* **2,** 476–486
11. Wells, C. M., Bhavsar, P. J., Evans, I. R., Vigorito, E., Turner, M., Tybulewicz, V., and Ridley, A. J. (2005) *Exp. Cell Res.* **310,** 303–310
12. Pearce, A. C., Senis, Y. A., Billadeau, D. D., Turner, M., Watson, S. P., and Vigorito, E. (2004) *J. Biol. Chem.* **279,** 53955–53962
13. Fujikawa, K., Miletic, A. V., Alt, F. W., Faccio, R., Brown, T., Hoog, J., Fredericks, J., Nishi, S., Mildiner, S., Moores, S. L., Brugge, J., Rosen, F. S., and Swat, W. (2003) *J. Exp. Med.* **198,** 1595–1608
14. Möller, A., Dienz, O., Hehner, S. P., Dröge, W., and Schmitz, M. L. (2001) *J. Biol. Chem.* **276,** 20022–20028
15. Costello, P. S., Walters, A. E., Mee, P. J., Turner, M., Reynolds, L. F., Prisco, A., Sarner, N., Zamoyska, R., and Tybulewicz, V. L. (1999) *Proc. Natl. Acad. Sci. U.S.A.* **96,** 3035–3040
16. Manetz, T. S., Gonzalez-Espinosa, C., Arudchandran, R., Xirasagar, S., Tybulewicz, V., and Rivera, J. (2001) *Mol. Cell Biol.* **21,** 3763–3774
17. Zhou, Z., Yin, J., Dou, Z., Tang, J., Zhang, C., and Cao, Y. (2007) *J. Biol. Chem.* **282,** 23737–23744
18. Tybulewicz, V. L., Ardouin, L., Prisco, A., and Reynolds, L. F. (2003) *Immunol. Rev.* **192,** 42–52
19. Graham, D. B., Robertson, C. M., Bautista, J., Mascarenhas, F., Diacovo, M. J., Montgrain, V., Lam, S. K., Cremasco, V., Dunne, W. M., Faccio, R., Coopersmith, C. M., and Swat, W. (2007) *J. Clin. Invest.* **117,** 3445–3452
20. Miletic, A. V., Graham, D. B., Montgrain, V., Fujikawa, K., Kloeppel, T., Brim, K., Weaver, B., Schreiber, R., Xavier, R., and Swat, W. (2007) *Blood* **109,** 3360–3368
21. Wilkinson, B., Koenigsknecht-Talboo, *J.*, Grommes, C., Lee, C. Y., and Landreth, G. (2006) *J. Biol. Chem.* **281,** 20842–20850
22. Malhotra, S., Kovats, S., Zhang, W., and Coggeshall, K. M. (2009) *J. Biol. Chem.* **284,** 24088–24097
23. Riteau, B., Barber, D. F., and Long, E. O. (2003) *J. Exp. Med.* **198,** 469–474
24. Villalba, M., Bi, K., Rodriguez, F., Tanaka, Y., Schoenberger, S., and Altman, A. (2001) *J. Cell Biol.* **155,** 331–338
25. Hornstein, I., Alcover, A., and Katzav, S. (2004) *Cell. Signal.* **16,** 1–11
26. Spurrell, D. R., Luckashenak, N. A., Minney, D. C., Chaplin, A., Penninger, J. M., Liwski, R. S., Clements, J. L., and West, K. A. (2009) *J. Immunol.* **183,** 310–318
27. Phillipson, M., Heit, B., Parsons, S. A., Petri, B., Mullaly, S. C., Colarusso, P., Gower, R. M., Neely, G., Simon, S. I., and Kubes, P. (2009) *J. Immunol.* **182,** 6870–6878
28. Hinshaw, J. E. (2000) *Annu. Rev. Cell Dev. Biol.* **16,** 483–519
29. Gomez, T. S., Hamann, M. J., McCarney, S., Savoy, D. N., Lubking, C. M., Heldebrant, M. P., Labno, C. M., McKean, D. J., McNiven, M. A., Burkhardt, J. K., and Billadeau, D. D. (2005) *Nat. Immunol.* **6,** 261–270
30. MacDonald, P. E., Eliasson, L., and Rorsman, P. (2005) *J. Cell Sci.* **118,** 5911–5920
31. Koncz, G., Kerekes, K., Chakrabandhu, K., and Hueber, A. O. (2008) *Cell Death Differ.* **15,** 494–503
32. van Tits, L. J., Hak-Lemmers, H. L., Demacker, P. N., Stalenhoef, A. F., and Willems, P. H. (2000) *Free Radic. Biol. Med.* **29,** 747–755
33. Kasri, N. N., Török, K., Galione, A., Garnham, C., Callewaert, G., Missiaen, L., Parys, J. B., and De Smedt, H. (2006) *J. Biol. Chem.* **281,** 8332–8338
34. Sun, B., Boyanovsky, B. B., Connelly, M. A., Shridas, P., van der Westhuyzen, D. R., and Webb, N. R. (2007) *J. Lipid Res.* **48,** 2560–2570
35. Collins, R. F., Touret, N., Kuwata, H., Tandon, N. N., Grinstein, S., and Trimble, W. S. (2009) *J. Biol. Chem.* **284,** 30288–30297
36. Lew, P. D., and Stossel, T. P. (1980) *J. Biol. Chem.* **255,** 5841–5846
37. Etzion, Y., Hackett, A., Proctor, B. M., Ren, J., Nolan, B., Ellenberger, T., and Muslin, A. J. (2009) *Circ. Res.* **105,** 148–157
38. Henry, P. D. (1990) *Am. J. Cardiol.* **66,** 3I–6I